TASK QUARTERLY 9 No 2, 187–198

UNSTEADY PERFORMANCE OF AN HP TURBINE STAGE OPTIMISED FOR STEADY FLOW CONDITIONS

JERZY ŚWIRYDCZUK

Institute of Fluid-Flow Machinery, Polish Academy of Sciences,
Fiszera 14, 80-952 Gdansk, Poland
jsk@imp.gda.pl

(Received 15 October 2004; revised manuscript received 23 November 2004)

Abstract: The article focuses on the examination of the unsteady performance of an HP turbine stage the blades of which were previously optimised for steady flow conditions. For the purpose of this examination, two pairs of initial and optimised stages of comparable output parameters were selected. The results have revealed that the modification of the blade profile in the optimisation process made the rotor blades more vulnerable to unsteady flow fluctuations, which eventually cancelled a considerable part of the stage efficiency gained from the steady flow optimisation.

Keywords: turbine stage, blade optimisation, unsteady effects

1. Introduction

Rapid developments in computer technology provide opportunities for modernisation of the turbine stage design process, in which the work of a human designer is replaced by an optimisation code. The code works in a loop, making decisions on further modifications of the stage geometry on the basis of the performance improvement resulting from changes previously introduced into the design. The bottle-neck of the entire optimisation process is the flow calculation, a time consuming component which, theoretically, has to be repeated for each newly generated version of the optimised stage. At present, optimisation methods of the highest efficiency are those making use of genetic algorithms to find a global solution in a way unaffected by local optima, along with neural networks to reduce the number of necessary flow calculations [1]. Despite those advanced methods, the optimisation methodology is still based entirely on steady flow calculations and does not take into account unsteady effects connected with the relative stator/rotor motion.

The goal of the present study is to detect the nature and scale of the inaccuracy introduced by the steady flow optimisation to the evaluation of performance characteristics of a stage working under unsteady flow conditions. For this purpose, the performance of two HP turbine stages has been examined. The first stage, referred to as initial, is a typical impulse turbine stage with cylindrical blades of standard

PLK and P2 profiles in the stator and the rotor, respectively, detailed characteristics of which can be found in the literature [2]. In the second stage the standard blading is replaced by blades that have been optimised on the basis of 2D steady flow calculations.

2. Stage geometry and numerical calculations

Basic dimensions of the stage in which the performance of the initial and optimised blading was examined were taken from an impulse turbine stage in operation. The stage geometry was simplified, see Figure 1, to avoid leakage flows and passage diameter changes, which were considered as side effects in the present study. The inner diameter of the passage, D_w, was equal to 812mm, while the blades' length, l, equalled 60mm. The stator-to-rotor pitch ratio, t_s/t_r, was 2.36. The assumed flow conditions were identical for all the examined cases. The total inlet pressure, P_{0c}, and temperature, T_{0c}, were 79bar and 746.3K, respectively. Static pressure, P_2, at the stage exit was 71bar. The direction of the flow at the stage inlet was assumed to be radial ($\alpha_0 = \gamma_0 = 0$).

Calculations of the stage's performance were carried out using FlowER, a specialised code developed for computing 3D viscous, compressible flows through individual stages and entire multistage turbine sections. The governing relations used in the code have the form of RANS (Reynolds-Averaged Navier-Stokes) equations for a thermodynamically perfect gas, complemented by a selected turbulence model. Among

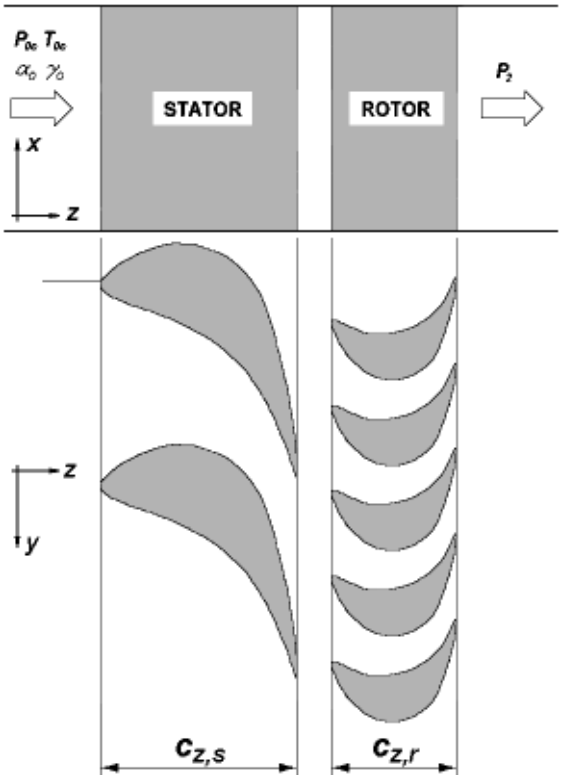

Figure 1. Initial stage geometry

other options, a modified Baldwin-Lomax model of turbulence is available, which assumes weighted averaging of turbulent viscosity values in the flow areas near wall intersections, and the SST (Shear Stress Transfer) model, developed by Menter [3], which combines two two-equation turbulence models: k-ε and k-ω, switching them on in the areas of their better applicability. The RANS equations are solved numerically using Godunov-type upwind differencing, accompanied by a high-resolution ENO (Essentially Non-Oscillatory) scheme for calculating convective derivatives. The computational efficiency is increased by implementing a multi-grid algorithm based on an H-type grid, refined near the walls and leading and trailing edges, along with the use of a δ-form implicit operator of Steger & Warming. The calculations are carried out in the computational area covering one passage in each turbine row. A more comprehensive description of the flow model and numerical procedure applied is given in [4, 5]. The code makes it possible, optionally, to calculate the course and effects of unsteady stator/rotor interactions by passing the entire flow field between the stator and rotor computational areas. In that case, the so-called time-space periodicity condition is assumed, a detailed description of which is given in [6].

The calculations discussed in the article were carried out on a grid with 244 608 and 337 792 cells in the stator and rotor computational areas, respectively. For unsteady variants, the number of 130 000 iterations at the third grid level covered almost 30 rotor periods, T, defined as time intervals during which a rotor blade rotates to cover the distance corresponding to the stator's pitch.

3. The turbine stage's steady flow characteristics

The optimisation introduced only minor changes to the shape of the stator blade profile. Generally, the profile's thickness increased in the front part of the blade and decreased in its rear part. A more regular distribution of flow parameters was obtained as a result. Figure 2a offers a comparison of the pressure and Mach number distributions recorded at the stator's mid-span sections of the two examined stages. The curves representing the initial blade reveal small wiggles, most likely due to the profile shape being given, by definition, as a set of arcs, tangential but not preserving the continuity of the second derivative at the points of contact. The optimised profile curves, marked with dashed lines, are visibly more regular.

The shape of the rotor blade profile was changed more dramatically in the optimisation process. An optimised blade has greater camber and a much sharper

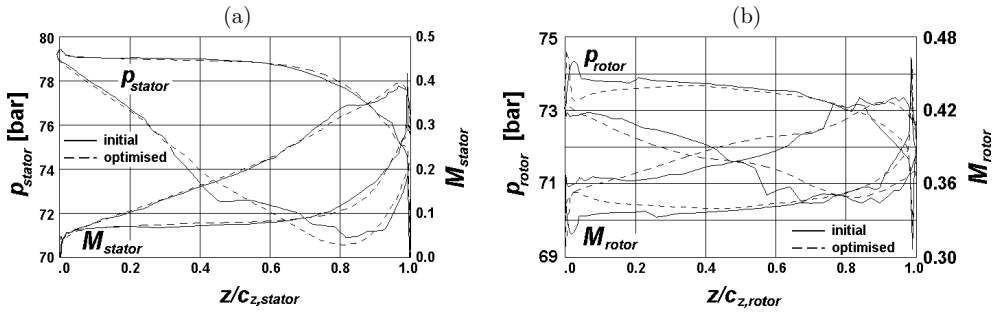

Figure 2. Static pressure and Mach number distributions around contours of stator (a) and rotor (b) blades

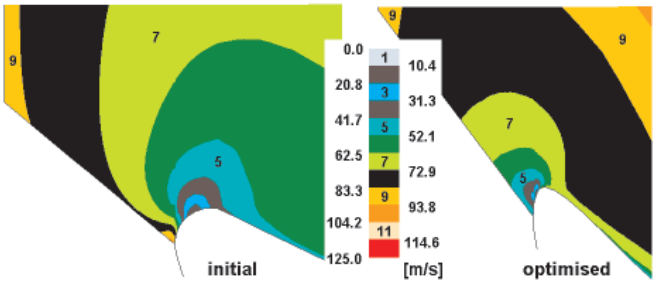

Figure 3. Constant velocity contours near rotor blades' leading edges

leading edge and is generally thinner. The resulting changes in rotor performance are also more pronounced. Like for the stator, the pressure and Mach number distributions over the profile contour of the optimised blade in the mid-span section are more regular (see Figure 2b). But in this case the two pairs of curves differ to a greater degree, especially in the vicinity of the blade's leading edge. Starting from the maximum pressure peak at the leading stagnation point static pressure decreases rapidly for the optimised blade and only at an approximate distance of $0.4C_z$ does it meet the initial stage curve. The corresponding velocity changes can be observed in the Mach number distributions.

A more regular flow velocity distribution in the rotor passage with optimised blades is also noticeable on the map of constant velocity contours shown in Figure 3. Here, it manifests itself by shorter distances between the neighbouring lines in the vicinity of the leading edge.

Apart from profile shapes, the optimisation process changed the rotor blades' stagger angle, which made it unclear what stagger positions of the initial and optimised rotor blades should be chosen to allow correct and reliable comparison. To select rotor positions securing their performance in comparable flow conditions, steady flow characteristics of the two stages were prepared. Two pairs of rotor stagger angles were selected on the basis of the collected material. One pair of rotors, denoted as 1A and 1B, was characterised by the axial direction of the flow leaving the rotor in the stator reference system (see Figure 4a). The other pair, denoted as 2A and 2B, was composed of rotors revealing the highest efficiency (see Figure 4b). In these two cases the difference in stagger angles of the initial and the optimised rotor was about 4 degrees. Rotor moments and mass flow rates are shown in Figures 4c and 4d to illustrate that the two selected rotor pairs operated under comparable flow conditions.

The results obtained for the initial rotor with blades at the nominal stagger angle were used as reference data in all diagrams.

Table 1. Kinetic energy loss changes (in %) due to blade optimisation

	1B–1A	2B–2A
Rotor loss	0.312	−0.213
Stage loss with exit velocity	−0.160	−0.396
Stage loss without exit velocity	−0.243	−0.401

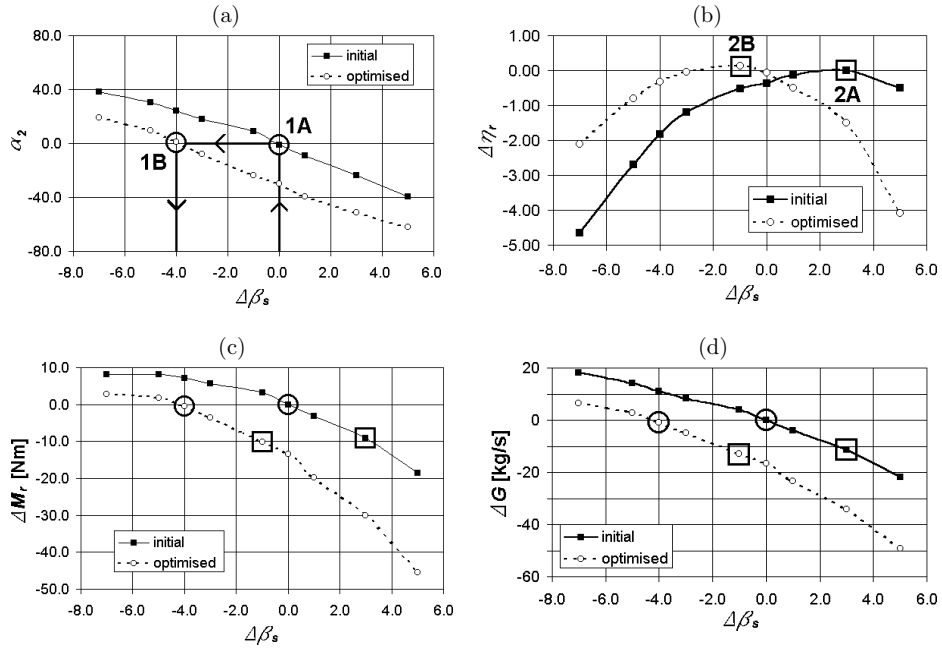

Figure 4. Rotor characteristics vs. rotor blades' stagger angle:
(a) flow exit angle; (b) efficiency; (c) blade moment; (d) mass flow rate

Differences in the efficiency of the corresponding rotor pairs, as evaluated from the steady flow calculations, have been collected in Table 1, presenting changes in the loss of kinetic energy, defined as $\zeta = \big(h_{1(2)} - h_{1s(2s)}\big)/(h_{0s} - h_{1s(2s)}) + \kappa_2$, where the h symbols respectively represent the enthalpy and isentropic enthalpy at the row (stage) exit and the stagnation enthalpy at the row (stage) inlet. The κ_2 term, taken into account in stage loss evaluation, stands for kinetic energy of the stream leaving the stage. A rotor loss increase amounting to 0.312 is noticeable for case 1, which suggests some vulnerability of the optimised rotor to off-optimum flow conditions.

4. Unsteady performance

The article discusses two aspects of unsteady effects generated by the stator/rotor interaction. One is the motion of stator wakes in the rotor cascade. Having shed from the trailing edges of stator blades, these wakes are chopped by rotor blades and their segments are transported with the flow through the rotor passages generating local disturbances in the distribution of flow parameters. The other aspect is connected with the geometry of the examined stage. Generally, when the stator/rotor pitch ratio, t_s/t_r, is sufficiently high, rotor blades may experience periodical fluctuations resulting from circumferential non-uniformity of the flow. In the examined stage $t_s/t_r = 2.36$, which means that only about 42% of the flow leaving a stator passage enters one rotor passage. In steady flow calculations, these two aspect are cancelled by circumferential averaging of flow parameters in the stator/rotor mixing plane and, consequently, they are neglected in numerical optimisations of the rotor blades.

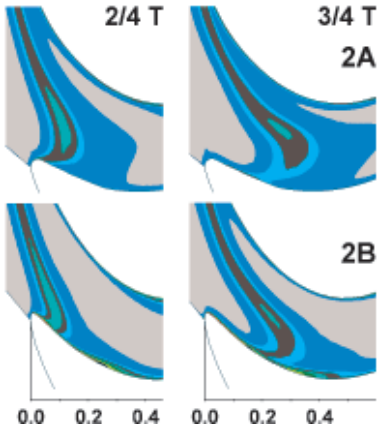

Figure 5. Wake patterns in the mid-span section

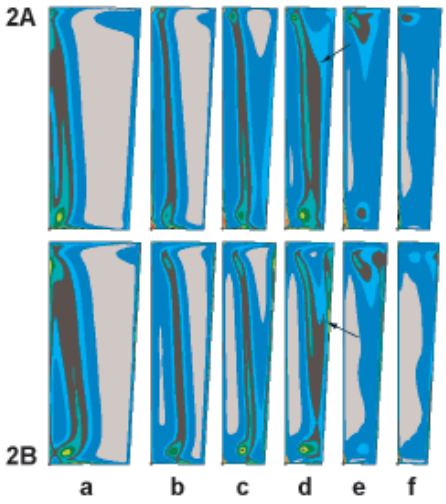

Figure 6. Wake patterns in $x0y$ sections; the wake's position corresponds to $3/4T$ from Figure 5

4.1. The stator wake's motion in the rotor passage

A common form of presenting the behaviour of the stator's wake in the rotor passage is showing instantaneous entropy distributions, most often in the mid-span section of the rotor passage. Areas of increased entropy in these distributions indicate instantaneous positions of the wake. This method has also been employed in the present article, cases 2A and 2B having been selected as the basic variants in the discussion. Figure 5 shows selected wake patterns in the mid-span sections of the stages for the times of $2/4T$ and $3/4T$. The diagrams for the first pair, $2/4T$, show the effect of different velocity distributions in front of the rotor on the wake's motion. The wake in passage 2A of the initial rotor is visibly more deformed on the blade pressure side. An interesting pattern of the flow through the optimised rotor is a small bubble on the blade pressure side, even more pronounced for time $3/4T$.

Figure 6, shows the $x0y$ sections of the wakes located at the instantaneous positions denoted by time $3/4T$. Particular a–f sections correspond to $z/c_{z,r} = 0.11$, 0.21, 0.32, 0.42, 0.50, and 0.60, respectively (see the scale in Figure 5). The inner structure of the two wakes is generally similar. An interesting pattern can be observed in d sections, which show the front parts of the wake. In both diagrams the wake's core has a tendency to widen (see the black contours indicated by the arrows) but for case 2B a secondary "limb" emerges from the main wake core at about 60% of its height. The remaining, upper part of the secondary core is located close to the pressure side of the passage.

For the same wake position, Figure 7 shows wake patterns at selected $y0z$ sections. In the 2B series the secondary limb has the form of a separation bubble interacting with the wake. Figure 8 explains the origin of the bubble, which turns out to separate from the blade's leading edge well before the wake approaches the

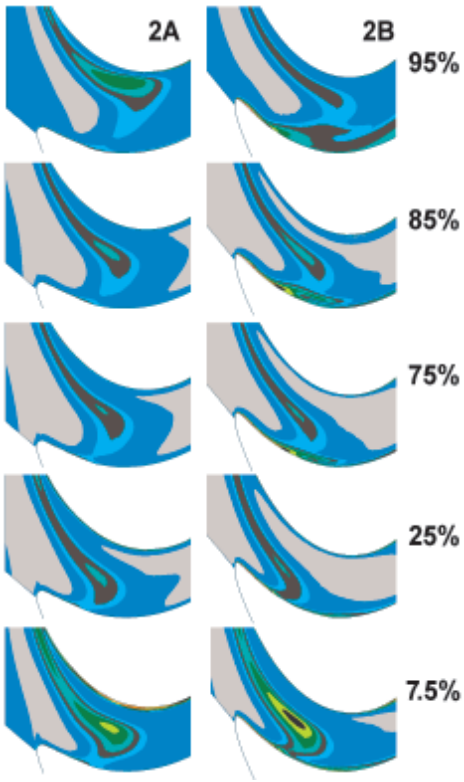

Figure 7. Wake patterns in $y0z$ sections; the wake's position corresponds to $3/4T$ from Figure 5

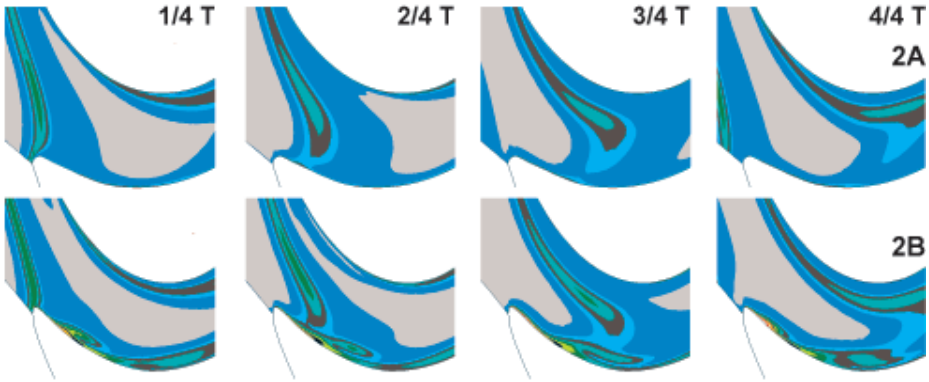

Figure 8. Instantaneous wake patterns in the $y0z$ section, $x/l = 87.5\%$

blade. The bubble then moves at a reduced speed along the blade's pressure side and is caught up by the wake, so that these two structures interact with each other.

In the initial stage data, the effect of flow separation is apparent in the 1B variant and almost unnoticeable in the 1A variant. This effect is rather of steady-state nature, resulting from an unfavourable angle at which the flow leaving the stator approaches the upper part of the rotor blade. From the point of view of the optimisation process, it is interesting to see how and to what extent this effect is

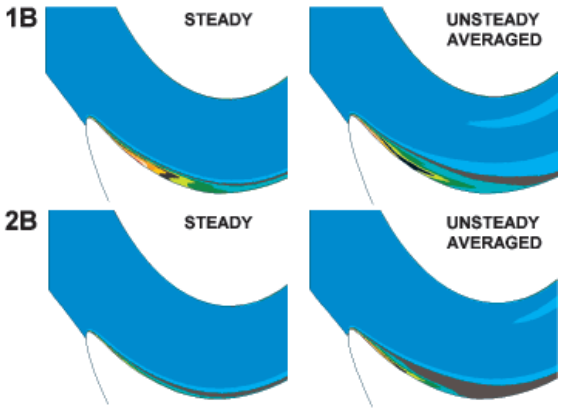

Figure 9. Flow separation in steady flow and unsteady calculations, $x/l = 87.5\%$

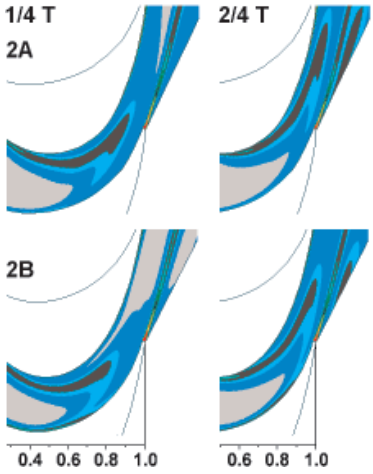

Figure 10. Wake patterns in the mid-span section, the rear part

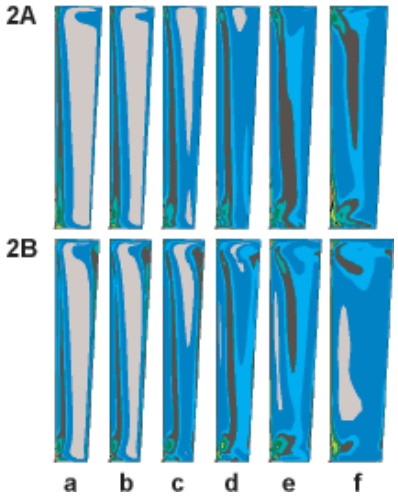

Figure 11. Wake patterns in $x0y$ sections, the wake's position corresponds to $1/4T$ from Figure 10

taken into account in steady flow calculations. Figure 9 gives a comparison of the flow separation patterns obtained from steady and unsteady flow calculations, the latter averaged over one period. The evident differences between these two cases are undoubtedly due to different rotor inlet flow conditions, which are averaged in the mixing plane in steady flow calculations.

The further development of the stator's wake on its way through the rotor passage is shown in Figures 10 and 11. The former presents the wake in the mid-span section recorded at times $1/4T$ and $2/4T$, while the latter shows the $x0y$ sections of the wake located at the instantaneous position denoted by time $\tau = 1/4T$. The general wake pattern is similar to that observed in the front part of the rotor passage. A new feature of the wake is its inclination towards the direction of the flow, resulting from the faster motion in the upper part of the passage. This tendency can be noticed by

observing locations of the wake core in the pairs of adjoining diagrams, e–f and d–e for cases 2A and 2B, respectively. The separation limb of the wake can be noticed in diagrams d–e for the 2B case, while slight tendencies towards separation can also be observed in the 2A e diagram.

The presented flow fields have been obtained using the modified Baldwin-Lomax model, which may raise questions about its effect on the final results. This problem has been examined by computing another 2B variant of unsteady flow through the optimised cascade using the two-equation SST model developed by Menter and comparing the results with those obtained for the Baldwin-Lomax model. An analysis of those results, given in detail in [7], suggests that flow field differences introduced by the two examined turbulence models are quantitative in nature and do not affect the general topology of the flow pattern. The most vulnerable flow areas are the hub sections of the rotor passages, in which the magnitudes and locations of the entropy peaks detected by the two turbulence models differ slightly. At the same time, both models have adequately predicted the flow separation in the upper part of the rotor passage, shown in Figure 8. The above results justify considering the tendencies presently observed in the flow patterns as real rather than generated by the turbulence model applied.

4.2. Non-uniformity of the flow

The flows in the stator/rotor gap of the examined stages exhibit velocity gradients in the circumferential direction. As a result, circumferential distributions of flow parameters vary with time at the rotor inlet. Velocity fluctuations recorded at the rotor's inlet range from about 60 m/s to nearly 110 m/s, while the flow angle changes are between 48° and 73°, as shown in Figure 12.

The changing flow conditions in the stator/rotor gap affect the inlet parameters in the rotor calculations. Figure 13 shows variations of the rotor inlet static pressure, circumferentially averaged in the mid-span section. In steady flow calculations this parameter is almost constant, after averaging in the mixing plane. It is also assumed to be constant in optimisation calculations performed for an individual stator or rotor row. The amplitudes in the table beside the figure are given in fractions of the static pressure drop in the stage. The curves in the diagram demonstrate that the amplitude of the pressure variations is equal to about 20% of the pressure drop, and it has been increased in the examined case due to the stage optimisation.

4.3. Efficiency changes

A crucial parameter in evaluating the effects of the optimisation process is the resulting level of loss. Figure 14 illustrates the process of the loss of kinetic energy building up in the rotor for the four examined cases. In all diagrams, the unsteady loss curves start at a level lower than their steady flow counterparts, but then rise rapidly to terminate at a significantly higher level at the rotor inlet. The different course of the build-up of kinetic energy loss in the stator/rotor gap is caused by numerical averaging of the flow parameters in the stator/rotor mixing plane in the steady flow calculations. A more detailed analysis of this effect and its impact on the loss evaluation is given in [8].

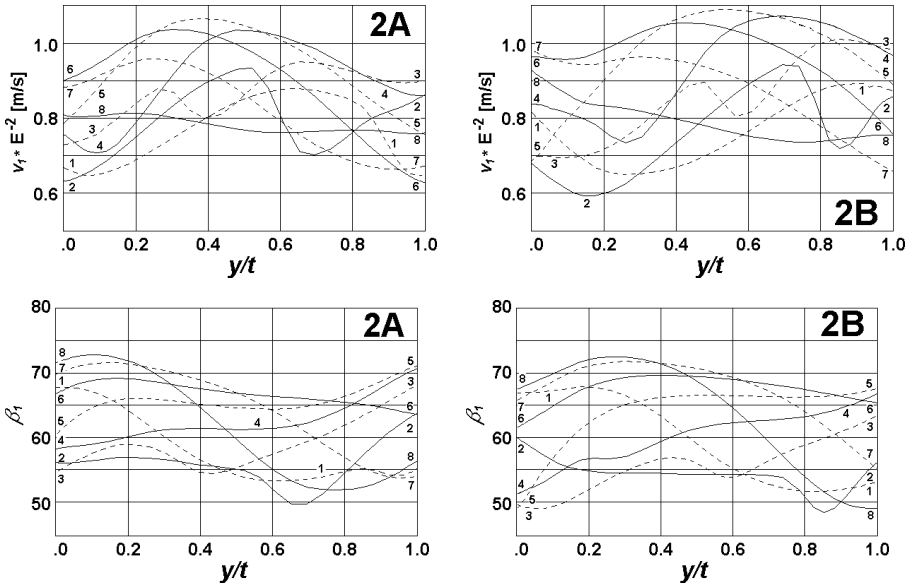

Figure 12. Instantaneous distributions of flow velocity and flow angle in the stator/rotor gap, the mid-span section, at a distance of 12% of c_x in front of the rotor cascade (flow velocity – top, flow angle – bottom); numbers 1, 2,..., 8 correspond to times $\tau = 1/8T$, $2/8T$,..., $8/8T$

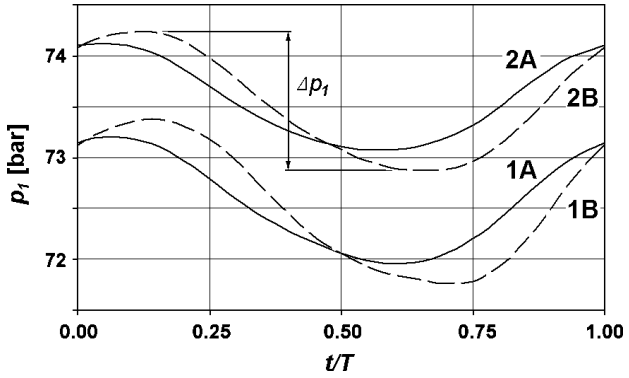

Figure 13. Variations of rotor inlet static pressure, circumferentially averaged in the mid-span section; $\Delta p_1/(p_2 - p_0) = 0.162$, 0.202, 0.132, and 0.172 for 1A, 1B, 2A, and 2B, respectively

In the direct vicinity of the rotor's leading edge the unsteady curves are even further moved towards higher losses and then reveal a relatively uniform shift with respect to the corresponding steady flow curves while the scale of the shift is slightly greater downstream of the rotor than inside the passage. This suggests that the most intensive generation of kinetic energy loss takes place in the vicinity of the rotor blades' leading and trailing edges. The observed shift is in principle more intensive for an optimised stage (case 1B or 2B) than for a corresponding initial stage (case 1A or 2A), which reveals a degree of vulnerability of an optimised rotor blade to flow changes. Table 2 summaries rotor and stage losses calculated at a distance of 80% of $C_{z,r}$ behind the rotor's trailing edge. In both cases, A and B, the stage performance improvement

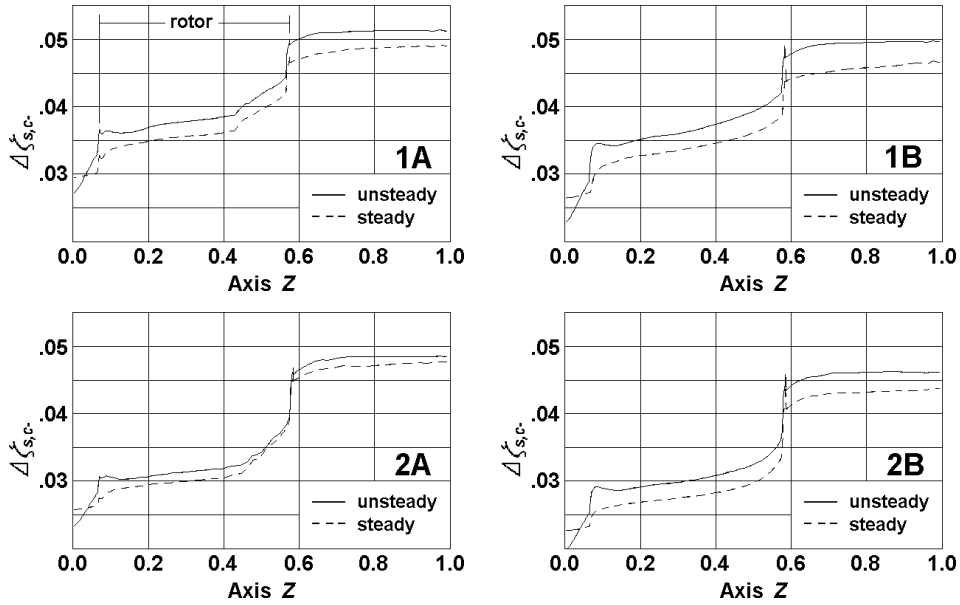

Figure 14. Kinetic energy loss build-up in the rotor along the turbine axis

Table 2. Comparison of unsteady and steady losses of kinetic energy in initial and optimised stages

	1B–1A	2B–2A
Rotor loss		
Steady	0.312	−0.213
Unsteady	0.719	0.281
Unsteady − Steady	0.407	0.494
Stage loss with exit velocity		
Steady	−0.160	−0.396
Unsteady	−0.102	−0.210
Unsteady − Steady	0.058	0.186
Stage loss without exit velocity		
Steady	−0.243	−0.401
Unsteady	−0.158	−0.235
Unsteady − Steady	0.085	0.166

obtained from steady flow optimisation is partially cancelled by unsteady effects. For case A the steady flow efficiency gain is reduced by about 35%, while in case B – by more than 40%. The data collected individually for the rotor reveals its vulnerability to flow fluctuations. The efficiency of the optimised rotor is higher only for the optimum stagger angle, case B and steady flow conditions, in all the remaining examined situations, both steady and unsteady, it performs poorer than the initial construction.

5. Conclusions

The presented performance study of the turbine stage with standard and optimised blades has revealed that shape modifications of the rotor blade profile introduced by the optimisation process made the rotor more vulnerable to unsteady flow fluctuations, which, in turn, cancelled a considerable part of the stage efficiency gained in the steady flow optimisation.

This conclusion is of significance for design tasks involving numerical optimisation. The present results indicate that automatic steady flow optimisation may produce blade shapes of improved characteristics only within a narrow range of parameters close to the ideal, uniform inlet flow. In real fluid-flow machines uniform flows do not occur, as they are always accompanied by unavoidable wakes shed from preceding rows and by other unsteady phenomena. An ideal solution to this problem would be optimisation based on unsteady flow calculations. Unfortunately, this approach cannot be applied at present due to extremely long times required by unsteady calculations. A good substitute solution would be an additional constraint in the optimisation process in the form of a minimum permissible blade leading edge radius, the exact value of which should be defined on the basis of the experience of human designers.

References

[1] Pierret S and Van den Braembussche R A 1999 *ASME J. Turbomachinery* **121** 326
[2] Deych M E, Filippov G A and Lazarev L J 1965 *Atlas of Axial Turbine Blade Profiles*, Mashinostrojenije, Moskva, USSR (in Russian)
[3] Menter F R 1994 *AIAA Journal* **32** 1598
[4] Yershov S V and Rusanov A V 1996 *The Application Package FlowER for the Calculation of 3D Viscous Flows Through Multistage Turbomachinery*, Certificate of Ukrainian State Agency of Copyright and Related Rights, Kiev, Ukraine
[5] Yershov S V, Rusanov A V, Gardzilewicz A, Lampart P and Świrydczuk J 1998 *TASK Quart.* **2** 319
[6] Rusanov A V and Yershov S V 1997 *Modelling and Design in Fluid-Flow Machinery* (Badur J, Bilicki Z, Mikielewicz J and Śliwicki E, Eds.), IMP PAN Publishing, Gdansk, Poland, pp. 153–160
[7] Świrydczuk J 2002 *Turbomachinery (Cieplne Maszyny Przepływowe)* **122** 269
[8] Gardzilewicz A and Świrydczuk J 2002 *Turbomachinery (Cieplne Maszyny Przepływowe)* **122** 321